Original Article

The hemodynamic and geometric characteristics of carotid artery atherosclerotic plaque formation

Na Han[1,2,3#], Jintao Wang[4#], Yurong Ma[1,2], Laiyang Ma[1,2,3], Yu Zheng[1,2,3], Fengxian Fan[1,2], Chuang Wu[1,2], Songhong Yue[1,2,3], Jie Li[1,2], Juan Liang[1,2], Hui Zhang[1,2], Yuxuan Zhou[1,2], Tingli Yang[1,2], Jing Zhang[1,2]

[1]Department of Magnetic Resonance, Lanzhou University Second Hospital, Lanzhou, China; [2]Gansu Province Clinical Research Center for Functional and Molecular Imaging, Lanzhou, China; [3]The Second Clinical Medical School, Lanzhou University, Lanzhou, China; [4]Department of Cardiovascular Medicine, Lanzhou University Second Hospital, Lanzhou, China

Contributions: (I) Conception and design: N Han, J Wang, J Zhang; (II) Administrative support: Y Ma, L Ma, Y Zheng, J Zhang; (III) Provision of study materials or patients: N Han, J Wang; (IV) Collection and assembly of data: F Fan, C Wu, S Yue, J Li; (V) Data analysis and interpretation: N Han, J Wang, J Liang, H Zhang, Y Zhou, T Yang; (VI) Manuscript writing: All authors; (VII) Final approval of manuscript: All authors.

[#]These authors contributed equally to this work.

Correspondence to: Jing Zhang, MD. Department of Magnetic Resonance, Lanzhou University Second Hospital, 82 Cuiyingmen, Chengguan District, Lanzhou 730030, China; Gansu Province Clinical Research Center for Functional and Molecular Imaging, Lanzhou, China. Email: ery_zhangjing@lzu.edu.cn.

Background: Ischemic stroke, which has a high incidence, disability, and mortality rate, is mainly caused by carotid atherosclerotic plaque. The difference in the geometric structures of the carotid arteries inevitably leads to the variability in the local hemodynamics, which plays a key role in the formation of carotid atherosclerosis. At present, the combined mechanisms of hemodynamic and geometric in the formation of carotid atherosclerotic plaque are not clear. Thus, this study characterized the geometric and hemodynamic characteristics of carotid atherosclerotic plaque formation using four-dimensional (4D) flow magnetic resonance imaging (MRI).

Methods: Ultimately, 122 carotid arteries from 61 patients were examined in this study. According to the presence of plaques at the bifurcation of the carotid artery on cervical vascular ultrasound (US), carotid arteries were placed into a plaque group (N=69) and nonplaque group (N=53). The ratio of the maximum internal carotid artery (ICA) inner diameter to the maximum common carotid artery (CCA) inner diameter (ICA-CCA diameter ratio), bifurcation angle, and tortuosity were measured using neck three-dimensional time-of-flight magnetic resonance angiography (3D TOF-MRA). Meanwhile, 4D flow MRI was used to obtain the following hemodynamic parameters of the carotid arteries: volume flow rate, velocity, wall shear stress (WSS), and pressure gradient (PG). Independent sample *t*-tests were used to compare carotid artery geometry and hemodynamic changes between the plaque group and nonplaque group.

Results: The ICA-CCA diameter ratio between the plaque group and the nonplaque group was not significantly different (P=0.124), while there were significant differences in the bifurcation angle (P=0.005) and tortuosity (P=0.032). The bifurcation angle of the plaque group was greater than that of the nonplaque group (60.70°±20.75° *vs.* 49.32°±22.90°), and the tortuosity was smaller than that of the nonplaque group (1.07±0.04 *vs.* 1.09±0.05). There were no significant differences between the two groups in terms of volume flow rate (P=0.351) and the maximum value of velocity (velocitymax) (P=0.388), but the axial, circumferential, and 3D WSS values were all significantly different, including their mean values (all P values <0.001) and the maximum value of 3D WSS (P<0.001), with the mean axial, circumferential, 3D WSS values, along with the maximum 3D WSS value, being lower in the plaque group. The two groups also differed significantly in terms of maximum PG value (P=0.030) and mean PG value (P=0.026), with these values being greater in the nonplaque group than in the plaque group.

Conclusions: A large bifurcation angle and a low tortuosity of the carotid artery are geometric risk factors for plaque formation in this area. Low WSS and low PG values are associated with carotid atherosclerotic plaque formation.

Keywords: Carotid artery; atherosclerotic plaque; four-dimensional flow magnetic resonance imaging (4D flow MRI); carotid geometry; hemodynamics

Submitted Dec 24, 2023. Accepted for publication May 08, 2024. Published online Jun 11, 2024.
doi: 10.21037/qims-23-1827
View this article at: https://dx.doi.org/10.21037/qims-23-1827

Introduction

The latest data from the Global Burden of Disease (GBD) study indicates that stroke is the primary cause of death and disability in adults in China, imposing a massive economic burden upon patients and society (1). Stroke can be divided into ischemic and hemorrhagic types. According to the latest statistical data in China, ischemic stroke accounts for about 70% of stroke cases, making it the most common type of stroke (2). Ischemic stroke refers to blockage of blood vessels in the brain or neck and interruption of cerebral blood flow supply that leads to nerve cell death and neurological dysfunction (3). Atherosclerosis is the most common cause of ischemic stroke. The common carotid artery (CCA) ascends from the aortic arch and branches into the internal and external carotid arteries. The internal carotid artery (ICA) system supplies the anterior two-thirds of the cerebral hemisphere and some parts of the diencephalon, thus providing about 70% of the blood to the brain (4). Carotid artery atherosclerosis or other diseases may reduce the cerebral blood supply due to carotid artery stenosis, thus leading to ischemic stroke (5). The formation mechanism of atherosclerotic plaque involves lipids in the blood accumulating under the vascular endothelium, macrophages phagocytizing lipid substances to form foam cells, smooth muscle cells migrating from the muscular layer to the subendothelium and transforming into fibroblasts, and subsequent occur necrosis, hemorrhage, calcification, and inflammatory changes (6). The primary mechanisms of ischemic stroke are the rupture of atherosclerotic plaque leading to thrombosis and the stenosis of the vascular lumen and hemodynamic changes caused by plaque (7).

Systemic arteries are subject to systemic risk factors of atherosclerosis, including age, gender, hyperlipidemia, hypertension, hyperglycemia, smoking, and obesity, but atherosclerosis plaque has specific predilection sites (8). The bifurcation of the CCA is the most common location of carotid atherosclerotic plaque, which is closely related to the geometric characteristics and hemodynamic factors of the bifurcation of the CCA (9). Therefore, identifying the potential geometric characteristics and hemodynamic that contribute to the formation of carotid artery plaques is highly relevant to the clinical context.

Hemodynamics is a branch of fluid mechanics that revolves around the mechanics of blood flow in the vascular system (10). In hemodynamics, bulk flow refers to the central part of the flow of blood in blood vessels, while wall shear stress (WSS) refers to the interaction at the interface of the blood flow and vessel wall (11). More specifically, WSS is the shear stress exerted by a fluid in the tangential direction on the wall, which determines the degree of interaction between the fluid and the wall (12). WSS can be divided into axial WSS and circumferential WSS. Axial is the direction of the central axis of the blood vessel, circumferential is the direction along the circumference of the blood vessel wall, and three-dimensional (3D) WSS is a combination of axial and circumferential WSS (13). Hemodynamic parameters include basic parameters such as blood flow velocity, volume flow rate, and advanced parameters such as WSS, pressure gradient (PG), wall pressure, pulse wave velocity (PWV), energy loss (EL), and turbulent kinetic energy (TKE) (14). Velocity is measured as the blood flow velocity through a given section in a unit of time, volume flow rate as a blood flow volume through a given section in a unit of time, WSS as the force of blood flow on the vessel wall along the tangent direction of the vessel, PG as a pressure change per unit distance, wall pressure as the mechanical pressure of blood flow acting perpendicular to the surface of the lumen PWV=$\Delta d/\Delta t$, where Δd represents the distance between two measurement planes within the blood vessel, and Δt represents the time shift of the flow velocity curve. EL as the ratio of lost energy to vessel volume in the deformation cycle, and TKE as the rapid velocity fluctuations within a single imaging voxel

independent of direction (i.e., a turbulence flow intensity measurement parameter), which can be used to evaluate the degree of blood flow turbulence and the severity of vascular lesions.

The early, more commonly used hemodynamic measurement techniques included ultrasound (US) and computational fluid dynamics (CFD), but US is not accurate in measuring advanced parameters. CFD can calculate flow fields at higher spatial and temporal resolution (15,16), but the accuracy is limited by the application of the fluid model and wall function, the precision of the boundary conditions, and the validity of the underlying assumptions (17-19). Four-dimensional (4D) flow magnetic resonance imaging (MRI) is a vascular imaging technique based on phase-contrast MRI (PC-MRI). It can directly measure highly comprehensive hemodynamic parameters *in vivo* from any direction and angle during different cardiac cycles and can visualize blood flow direction and condition (20). 4D flow MRI has been widely used in large blood vessels of the heart, with relatively few applications for the head and neck blood vessels.

Research suggests that the geometric characteristics of the common carotid bifurcation play a role in the formation of atherosclerosis by influencing hemodynamics and are potential imaging markers for predicting the risk of atherosclerosis (21). The commonly used parameters for evaluating the geometric characteristics of the carotid artery include the ratio of the maximum ICA inner diameter to the maximum CCA inner diameter (ICA-CCA diameter ratio), bifurcation angle, and tortuosity. Although these geometric parameters are key independent predictors of early carotid artery wall thickening and plaque formation (22), they are not widely accepted in clinical practice and not included in clinical decision-making.

Therefore, to further clarify the hemodynamic and geometric mechanisms of carotid atherosclerotic plaque formation, we aimed to characterize the combined geometric and hemodynamic characteristics of carotid atherosclerotic plaque formation using 4D flow MRI. We present this article in accordance with the STROBE reporting checklist (available at https://qims.amegroups.com/article/view/10.21037/qims-23-1827/rc).

Methods

This study was conducted in accordance with the Declaration of Helsinki (as revised in 2013) and was approved by The Ethics Committee of the Second Hospital of Lanzhou University (No. 2024A-616). Informed consent was taken from all participants.

Participants

We recruited 73 patients with unilateral or bilateral carotid plaques from August 2022 to August 2023, with 12 patients with low-quality imaging being excluded from the study. Ultimately, 122 carotid arteries from 61 patients were examined. Among the patients, 8 had plaque in the bilateral carotid arteries, and 53 had plaque in the unilateral carotid artery. Among the carotid arteries, 69 had plaques (32 left carotid arteries with plaque and 37 right carotid arteries with plaque), and 53 had no plaque (29 nonplaque left carotid arteries and 24 nonplaque right carotid arteries).

Examination protocol

All patients underwent neck vascular US, three-dimensional time-of-flight magnetic resonance angiography (3D TOF-MRA), and 4D flow MRI examinations. Moreover, 12 patients underwent high-resolution vascular wall MRI of the head and neck.

An iU22 ultrasonic diagnostic apparatus (Philips, Amsterdam, the Netherlands) was used to perform standard scanning on the transverse and longitudinal sections of the bilateral CCA, ICA, and external carotid artery of a population at high risk of atherosclerosis. This population included those with risk factors of hypertension, hyperlipidemia, hyperglycemia, coronary heart disease, smoking, alcoholism, obesity, and family history of atherosclerosis. Those with ≥3 risk factors and over 40 years old were required to undergo neck vascular US examinations regularly.

The position, size, and echo of the carotid atherosclerotic plaque scanned were recorded, and the plaque surface and shape were observed. The absorption and reflection of sound waves vary among different the components of carotid artery plaque, resulting in different grayscale US manifestations of carotid artery plaque. With the vascular wall as a reference, the normal vascular wall has three layers of echogenicity: moderate echogenicity (inner membrane layer), low echogenicity (middle membrane layer), and high echogenicity (outer membrane layer; posterior without acoustic shadows). The echo is the same as that of the bone, and plaque with posterior acoustic shadows is considered to be strongly echogenic plaque (calcified plaque). According to the internal echo of the plaque, carotid artery plaques can be divided into the following three categories: (I)

hypoechoic plaques, the echo inside the plaque is lower than that in the intimal layer of the blood vessel wall; (II) isoechoic plaques, the echo within the plaque is relatively consistent with the echo of the intimal layer of the blood vessel wall, and (III) hyperechoic plaques, the echo within the plaque is equal to or slightly higher than that of the outer membrane layer of the blood vessel wall. Two-dimensional grayscale US indicates homogeneous echogenic plaque if the internal echoes are uniform and consistent; meanwhile, it indicates heterogeneous echogenic plaque if more than 20% of the echoes are inconsistent within the plaque (23). Research (24-26) has shown that carotid artery plaque with an uneven surface, irregular shape, low echogenicity, and mixed echogenicity is mainly unstable, while that with a smooth surface, regular appearance, and high echogenicity is mostly stable. In this study, patients with stable plaque at the bifurcation of the unilateral or bilateral common carotid arteries were included. The evaluation criteria for stable plaque were as follows: (I) protruding from the vascular lumen or with a focal intima-media thickness (IMT) ≥1.5 cm and greater than 50% of the surrounding IMT; and (II) a regular morphology, smooth surface, and a homogeneous high echogenicity or isoechogenicity.

The 4D flow MRI and 3D TOF-MRA scans were performed using a 3.0 T MRI scanner (Ingenia CX, Philips) with a 32-channel head-neck coil. The 4D flow MRI was acquired using a volumetric and a time-resolved PC method. The scanning parameters were as follows: repetition time (TR) =5.6 ms, echo time (TE) =3.0 ms, flip angle=8°, field of view (FOV) =200 mm × 200 mm × 50 mm, matrix size =200×200, slice number =50 (axial), Slice thickness =1 mm, ACQ (acquisition) voxel size =1 mm × 1 mm × 1 mm, recon (reconstruction) voxel size =0.391 mm × 0.391 mm × 1mm, and velocity encoding (VENC) =100 cm/s. 4D flow MRI scanning requires patients to wear a finger pulse clamp for capturing real-time dynamic changes in hemodynamics during the cardiac cycle. After scanning, three phase maps representing three directions and an amplitude map were obtained. The total scan time of the 4D flow was approximately 16 minutes depending on the heart rate of the participants. Twenty frames were reconstructed through view sharing.

3D TOF-MRA utilizes the inflow enhancement effect of flowing blood in gradient echo sequences for vascular imaging, which is a noncontrast vascular imaging technique. The scanning parameters were as follows: TR =17 ms, TE =3.5 ms, flip angle =18°, FOV =190 mm × 190 mm × 104 mm, matrix size =344×216, slice number =160, slice thickness =20 mm, and voxel size =0.55 mm × 0.88 mm × 1.3 mm. The total scan time was 1 minute and 32 seconds.

Image analysis

Measurement of the carotid artery geometry was conducted via 3D TOF-MRA as displayed in *Figure 1*. The measured geometric parameters included the following: (I) ICA-CCA diameter ratio, the ratio of the ICA maximum inner diameter to the CCA maximum inner diameter; (II) bifurcation angle, the two tangent lines along the outer wall of internal and external carotid arteries (denoted as α); and (III) tortuosity of the carotid artery, the distance along the center of the CCA-ICA lumen (with the starting and ending points being 1 cm above and below the bifurcation of the carotid artery) divided by the straight distance of the CCA-ICA lumen center (with the starting and ending points being 1 cm above and below the bifurcation of the carotid artery).

The procedure for 4D flow MRI processing is displayed in *Figure 2*. 4D flow MRI data were imported into the CVI42 v. 5.14 software (Circle Cardiovascular Imaging, Calgary, AB, Canada) for processing and parameter measurement. The processing steps included the following: (I) preprocessing, including automatic offset correction and antialiasing to identify and remove low-quality images; (II) segmentation, including the segmentation of the target blood vessels along their centerline; and (III) analysis, including visualization and quantitative analysis. In quantitative analysis, the analyzed plane is placed perpendicular to the bifurcation of the CCA, and the lumen contour in the amplitude image is manually adjusted to improve the accuracy of the measurement. At this moment, the color coded axial and sagittal images are visualized. The measured hemodynamic parameters included the following: volume flow rate, maximum velocity ($velocity_{max}$), axial mean WSS (WSS_{mean}), circumferential WSS_{mean}, 3D maximum WSS (WSS_{max}), 3D WSS_{mean}, maximum PG (PG_{max}), and mean (PG_{mean}). Velocity, vector, pathline, and streamline visualization was performed.

Interobserver and intraobserver consistency analysis

Forty carotid arteries were randomly selected to test the interobserver and intraobserver reproducibility via intraclass correlation coefficients (ICC). Observer 1 and observer 2 separately evaluated the 40 randomly selected carotid

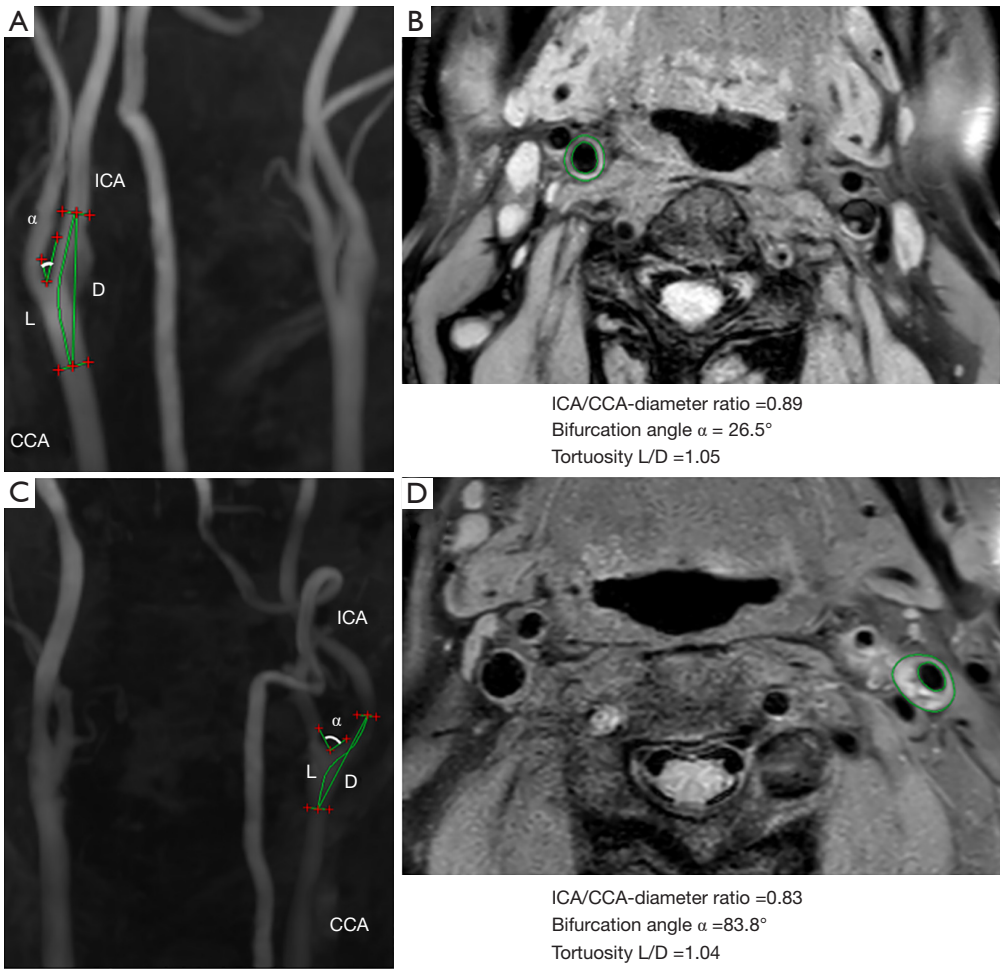

Figure 1 Measurement of the geometric characteristics of the carotid artery. (A) 3D TOF-MRA. (B) High-resolution vessel wall magnetic resonance imaging. (A,B) Images of the same patient showing the bifurcation of the bilateral carotid arteries without plaque. (C) 3D TOF-MRA. (D) High-resolution vessel wall magnetic resonance imaging. (C,D) Images of the same patient showing the bifurcation of the left carotid artery with plaque. ICA, internal carotid artery; CCA, common carotid artery; α represent bifurcation angle; L, the distance along the center of the CCA-ICA lumen, with the starting and ending points being 1 cm above and below the bifurcation of the carotid artery; D, the straight distance of the CCA-ICA lumen center, with the starting and ending points being 1 cm above and below the bifurcation of the carotid artery; 3D TOF-MRA, three-dimensional time-of-flight magnetic resonance angiography.

arteries (including the carotid artery geometric and 4D flow MRI hemodynamic parameters), with ICC >0.75 indicating good interobserver consistency. Observer 1 reanalyzed the 40 randomly selected carotid arteries one month after initial analysis, with ICC >0.75 indicating good intraobserver consistency.

Statistical analysis

All statistical analyses were performed using the GraphPad Prism 9.5.1 (GraphPad Software, Inc., La Jolla, CA, USA). Classification variables are represented as frequencies and percentages. According to the normality test, all continuous variables corresponded to a normal distribution. Therefore, continuous variables are represented as the mean ± standard deviation. The independent samples *t*-test was used to compare continuous variables between two groups. A violin chart was used to visualize the distribution of continuous variables. P<0.05 was considered to indicate a statistically significant difference.

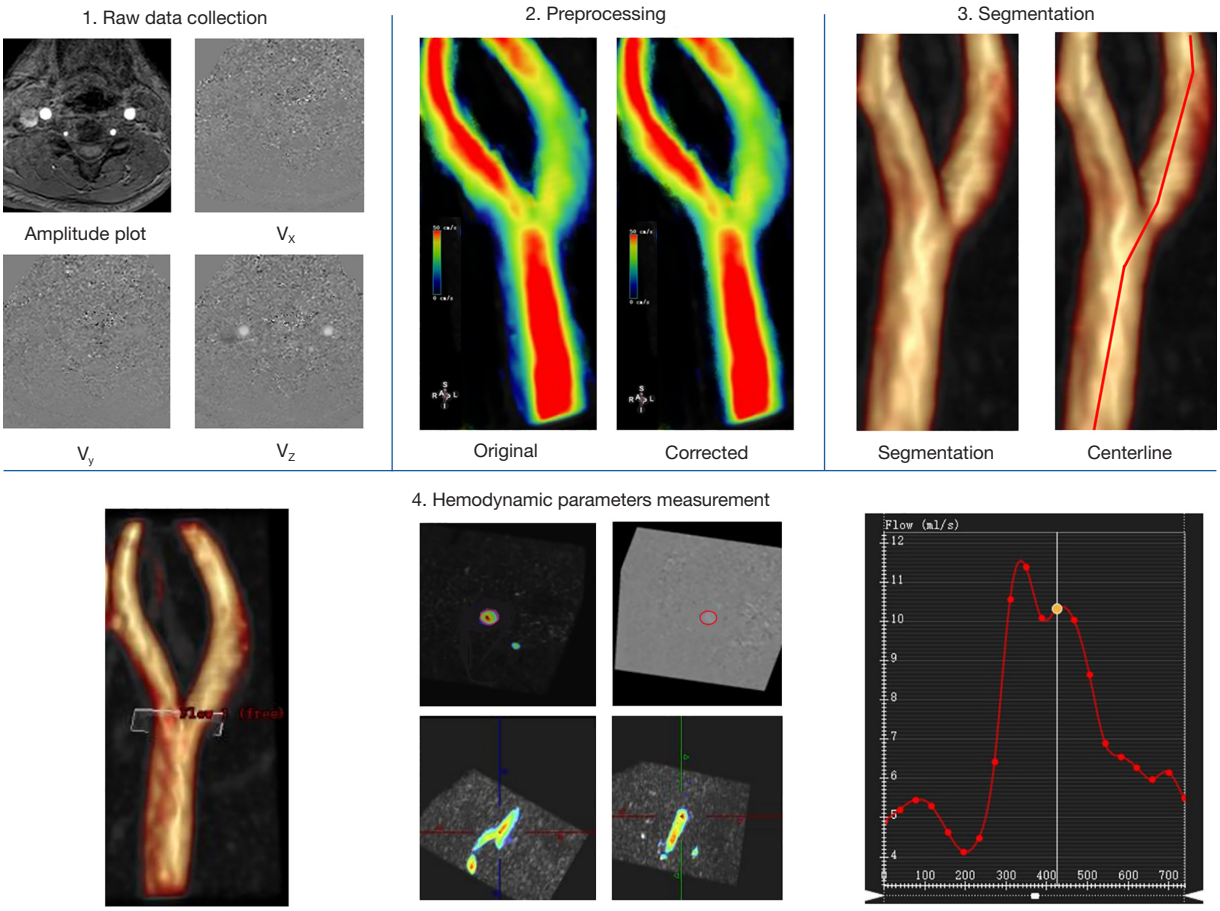

Figure 2 Four-dimensional flow MRI hemodynamic parameter measurement flowchart. A plane was placed in the bifurcation of the common carotid artery (left first of lower row), and every plane was divided into several voxels. The volume flow rate was defined as the mean volume flow rate of all voxels. The 20 time points represent different times of cardiac cycles (right panel of the lower row). The volume flow rate of this plane was the mean volume flow rate at 20 time points. MRI, magnetic resonance imaging.

Results

Demographic characteristics

The demographic characteristics of the 61 patients are listed in *Table 1*. The 122 carotid arteries from these 61 patients were divided into a plaque group (N=69) and nonplaque group (N=53). Among the 61 patients (mean age 61.9±8.9 years), 31 were male, 30 were smokers, 30 had hypertension, 32 had diabetes, and 22 patients had hyperlipidemia. The mean heart rate was 69.7±11.1 times/min.

Geometric characteristics of the carotid artery among the plaque group and nonplaque group

The geometric characteristics of the carotid artery among plaque group and nonplaque group are displayed in *Table 2*. The difference in the ICA-CCA diameter ratio between the plaque group and the nonplaque group was not statistically significant (P=0.124), while there were significant differences in bifurcation angle (P=0.005) and tortuosity (P=0.032), as shown in *Figure 3*, with the bifurcation angle of the plaque group being greater than that of the nonplaque group (60.70±20.75° *vs.* 49.32±22.90°) and the tortuosity being smaller (1.07±0.04 *vs.* 1.09±0.05).

Hemodynamic changes in the plaque group and nonplaque group

The hemodynamic changes in the plaque group and nonplaque group are summarized in *Table 2*. The plaque

group and the nonplaque group showed no significant difference in volume flow rate (P=0.351) or velocity$_{max}$ (P=0.388). However, there were significant differences in the axial, circumferential, and 3D WSS, including the axial, circumferential, and 3D WSS$_{mean}$ (all P values <0.001) and the 3D WSS$_{max}$ (P<0.001). There were also significant differences in the PG$_{max}$ (P=0.030) and PG$_{mean}$ (P=0.026), as displayed in *Figure 4*. The axial WSS$_{mean}$, circumferential WSS$_{mean}$, 3D WSS$_{max}$, and 3D WSS$_{mean}$ of the plaque group were lower than those of the nonplaque, as were the PG$_{max}$ and PG$_{mean}$. *Figure 5* shows the velocity, vector, pathline, streamline, and WSS maps of the plaque group and nonplaque group.

Table 1 Patient demographic data

Characteristic	Value
Patient characteristic*	
Age (years)	61.9±8.9
Male	31 (50.8)
Smoking	30 (49.2)
Hypertension	30 (49.2)
Diabetes	32 (52.5)
Hyperlipidemia	22 (36.1)
Heart rate (times/min)	69.7±11.1
Plaque identification†	
With plaque	69
Without plaque	53

Data are presented as mean ± standard deviation, number (%) or number. *, for the entire cohort of 61 patients; †, for the 122 carotid arteries (69 plaque and 53 nonplaque).

Discussion

In this study, we finally included 61 patients with unilateral or bilateral carotid atherosclerotic plaques and analyzed the correlation between the geometric characteristics and hemodynamic parameters of 122 carotid arteries and the formation of plaques at the bifurcation of the CCA.

The common carotid bifurcation angle and the tortuosity of the ICA were found to be the major geometric factors for the formation of atherosclerotic plaque in the common carotid bifurcation area. The larger the bifurcation angle and the lower the tortuosity are, the more likely plaque formation is to occur. A longitudinal study showed that in the absence of ICA stenosis, the larger the bifurcation angle of the CCA is, the thicker

Table 2 Geometric characteristics and hemodynamics parameters of the carotid arteries

Parameters	Plaque group (N=69)	Nonplaque group (N=53)	P
Geometric characteristics			
ICA-CCA diameter ratio	0.74±0.12	0.78±0.15	0.124
Bifurcation angle (°)	60.70±20.75	49.32±22.90	0.005
Tortuosity	1.07±0.04	1.09±0.05	0.032
Hemodynamics			
Volume flow rate (mL/s)	4.99±1.43	5.22±1.17	0.351
Velocity$_{max}$ (cm/s)	45.06±10.60	46.69±9.91	0.388
Axial WSS$_{mean}$ (Pa)	0.23±0.06	0.29±0.07	<0.001
Circumferential WSS$_{mean}$ (Pa)	0.15±0.04	0.18±0.04	<0.001
3D WSS$_{max}$ (Pa)	0.25±0.08	0.33±0.13	<0.001
3D WSS$_{mean}$ (Pa)	0.16±0.05	0.22±0.10	<0.001
PG$_{max}$ (Pa)	0.47±0.19	0.55±0.21	0.030
PG$_{mean}$ (Pa)	0.21±0.09	0.25±0.11	0.026

Data are presented as mean ± standard deviation. ICA, internal carotid artery; CCA, common carotid artery; WSS, wall sheer stress; PG, pressure gradient.

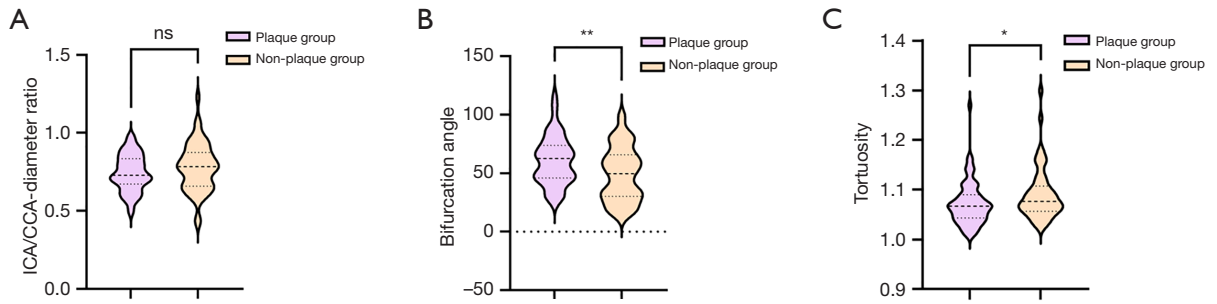

Figure 3 Geometric characteristics of the carotid artery among the plaque group and nonplaque group. (A) ICA/CCA-diameter ratio among the plaque group and nonplaque group. (B) Bifurcation angle among the plaque group and nonplaque group. (C) Tortuosity among the plaque group and nonplaque group. *, P<0.05; **, P<0.01. ns, no statistically significant difference; ICA, internal carotid artery; CCA, common carotid artery.

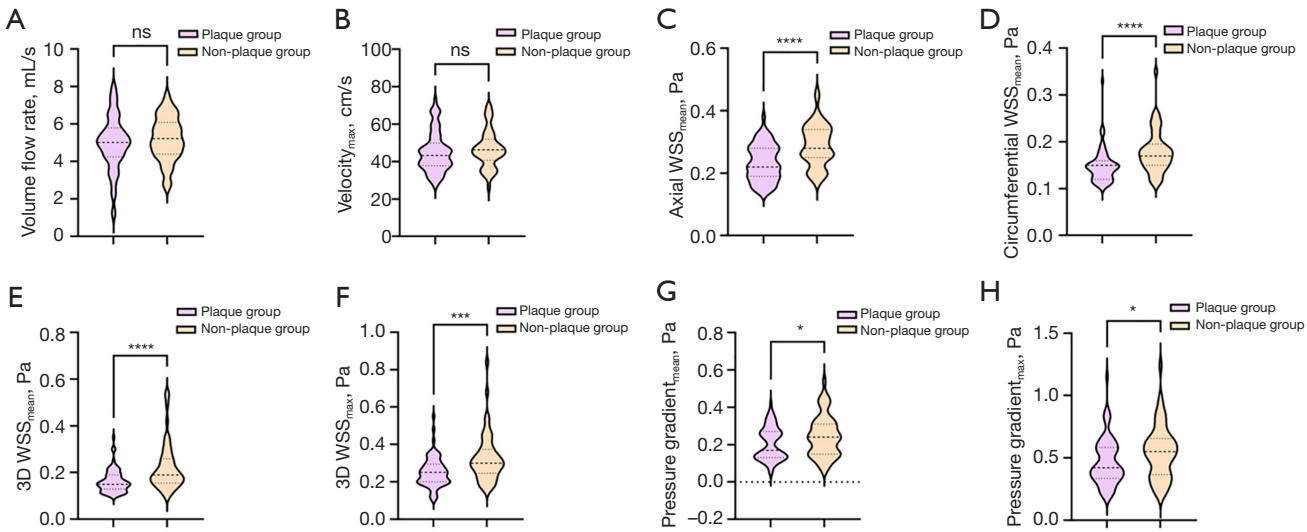

Figure 4 Hemodynamic changes among the plaque group and nonplaque group. (A) Volume flow rate among the plaque group and nonplaque group. (B) Velocity$_{max}$ among the plaque group and nonplaque group. (C) Axial WSS$_{mean}$ among the plaque group and nonplaque group. (D) Circumferential WSS$_{mean}$ among the plaque group and nonplaque group. (E) 3D WSS$_{mean}$ among the plaque group and nonplaque group. (F) 3D WSS$_{max}$ among the plaque group and nonplaque group. (G) PG$_{mean}$ among the plaque group and nonplaque group. (H) PG$_{max}$ among the plaque group and nonplaque group. *, P<0.05; ***, P<0.001; ****, P<0.0001. ns, no statistically significant difference; 3D, three-dimensional; WSS, wall shear stress; PG, pressure gradient.

the vascular wall thickness over time, which is an independent risk factor for carotid atherosclerotic plaque formation (27). This is similar to the conclusion of Bijari *et al.* (28), who found that the lager bifurcation angle of the carotid artery is a predictive indicator of vessel wall thickening at the early stage of atherosclerosis. Phan *et al.* (29) analyzed computed tomography angiography (CTA) images of 178 patients, reporting that geometric characteristics and anatomical structure were independent of traditional vascular risk factors for carotid artery stenosis. In addition, they demonstrated that the bifurcation angle was independently positively correlated with ICA near the CCA bifurcation stenosis, and that the greater the bifurcation angle was, the narrower the ICA near the CCA bifurcation was. This indirectly indicates that a larger bifurcation angle is more conducive to plaque formation of the ICA near the CCA bifurcation. The bifurcation angle influencing hemodynamics is the fundamental cause of this

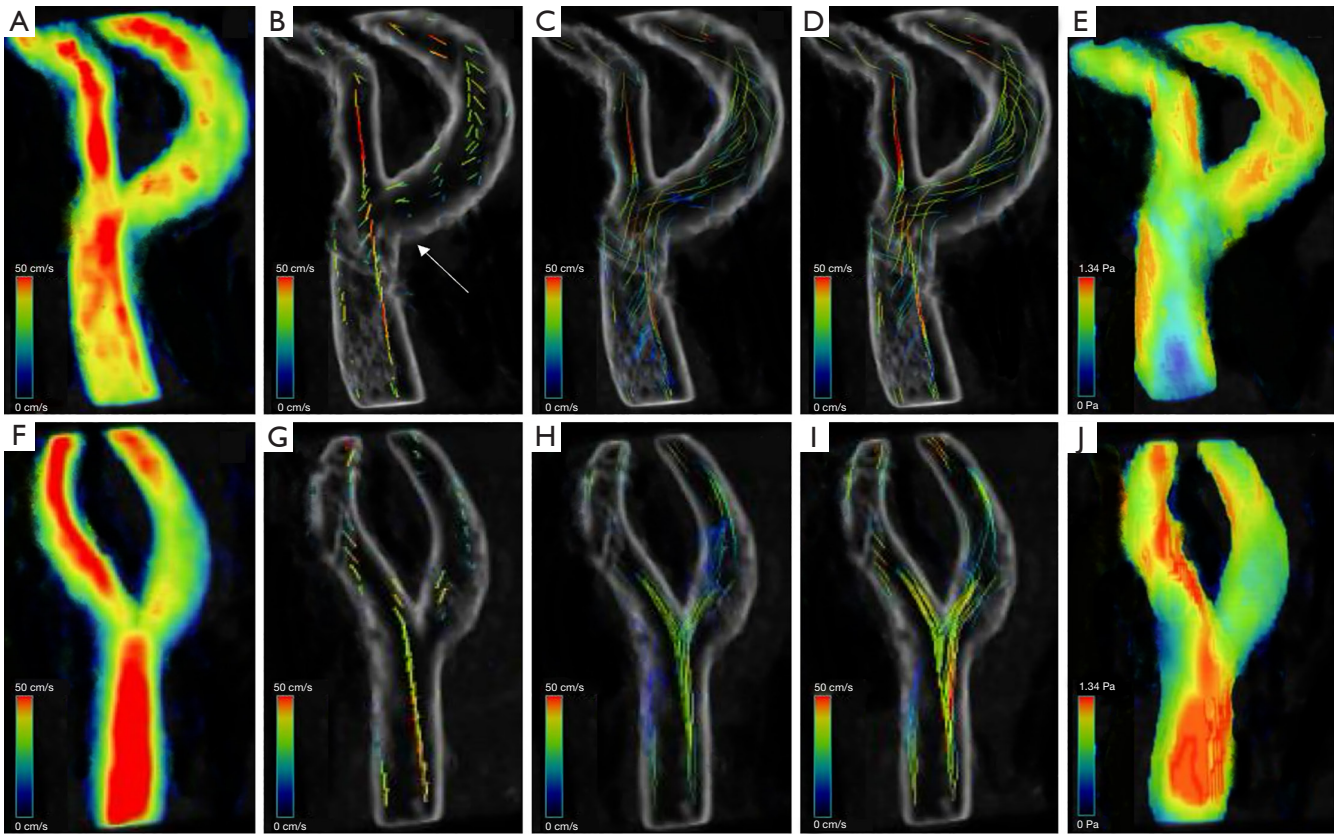

Figure 5 Visualization of the velocity, vector, pathline, streamline, and WSS maps from left to right, respectively. Upper row (A-E): the bifurcation of the carotid artery with plaque (as indicated by the arrow). Lower row (F-J): the bifurcation of the carotid artery without plaque. WSS, wall shear stress.

phenomenon, and previous CFD studies have proven that a greater bifurcation angle is associated with greater disorder in the blood flow in this area, with this in turn promoting the formation of atherosclerosis (30-32).

In our study, we also found that high ICA tortuosity exerted a protective effect for patients with carotid atherosclerosis, as high ICA tortuosity can delay or prevent the formation of atherosclerotic plaque by increasing spiral flow and reducing disturbed flow (33). A previous study on the data set of 50 models of human carotid bifurcation showed that intense spiral blood flow can inhibit the blood flow disturbance at the carotid bifurcation and that high carotid artery tortuosity contributes to the occurrence and development of spiral flow patterns, thus preventing the formation of atherosclerotic plaque (34). This is consistent with the results of another CFD study, which showed that a high tortuosity of the internal carotid and coronary arteries can prevent atherosclerosis by suppressing "disturbed flow" and increasing spiral flow (35,36). Research also indicates that helical characteristics and use of high-tortuosity stents to induce laminar and helical flow can prevent the formation of atherosclerotic plaque and reduce the probability of vascular restenosis (37-39). Strecker *et al.* reported that higher tortuosity indeed has a protective effect for patients with existing carotid artery stenosis and can reduce the risk of vascular restenosis (27). Other studies have indicated that the increase of spiral flow can reduce the deposition of low-density lipoprotein—a substance that contributes to atherosclerosis—in the vascular wall (40,41).

We further found that the ICA-CCA-diameter ratio of the plaque group was lower than that of the nonplaque group, which is similar to the results of Phan *et al.* (29), who reported a decrease in ICA-CCA-diameter ratio to be associated with the development of carotid artery stenosis. A baseline analysis of a study population also found a decrease in ICA-CCA-diameter ratio to be an independent predictor of an increase in carotid artery wall thickness (42). Additionally, an *in vivo* CFD study involving

both patients and volunteers demonstrated that disturbed flow is enhanced by local expansion of ICA spheres (21). Therefore, atherosclerosis is prone to occur at the carotid bifurcation. Although we found that the ICA-CCA-diameter ratio of the plaque group was lower than that of the nonplaque group, the difference was not statistically significant, which may be related to the sample size.

Our results also suggest that the geometry of the carotid artery is an important risk factor for the early development of atherosclerosis and plaque formation, which can be primarily attributed to the geometry of the carotid artery exerting an effect on hemodynamics. 4D flow MRI facilitates the measurement of all hemodynamic parameters with excellent temporal and spatial resolution (43). We used 4D flow MRI technology to evaluate the hemodynamic condition of the carotid artery in a plaque group and the nonplaque group. The analysis results showed that values of the axial, circumferential, and 3D WSS_{mean}, as well as 3D WSS_{max}, in the plaque group were significantly lower than those in the nonplaque group.

The WSS value is associated with degeneration and weakening of the artery wall's elastic fibers, as well as extracellular matrix imbalance. Low WSS is widely believed to significantly contribute to plaque formation and to initiate the atherosclerotic cascade reaction (44). Long-term investigation discovered that low WSS at baseline is an independent predictor of long-term increased carotid artery wall thickness (45). An investigation using US and a 12-year follow-up found that 48 patients experienced plaque growth in a location with low WSS (46). The cause of plaque formation may be a decrease in blood flow velocity, which prolongs the residence time of blood in the blood vessels, leading to persistent interactions between lipids and the vascular wall (47). Research indicates that low WSS can increase the uptake of low-density lipoprotein, leading to the formation of lipid components in plaque; in addition, low WSS values directly affect the vascular endothelium (48). Cumulatively, these reactions promote the development of atherosclerosis. Meanwhile, studies have found that after the formation of atherosclerotic plaque, high WSS can cause certain alterations in endothelial cell behavior, exacerbate inflammation, stimulate the progress of atherosclerotic lipid core in the vascular wall, and contribute critically to the factors that trigger vulnerability to plaque formation and final rupture (49).

In addition, some studies (21,22,27) have shown that the carotid bifurcation angle is negatively correlated with WSS, while the tortuosity is positively correlated with WSS; that is, a large carotid bifurcation angle and low tortuosity are correlated with low WSS, and they are independent predictors of atherosclerotic plaque formation, which is consistent with the results of our study. A study using CFD and MRI on 13 patients undergoing carotid artery surgery showed that a larger carotid bifurcation angle results in a lower WSS, which was found to cause vascular restenosis in a 5-year follow-up (50).

Few studies have used PG value to detect plaque formation. In our study, we discovered that the nonplaque group's PG_{max} PG_{mean} values were significantly higher than those of the plaque group. Another study compared the PG value between healthy participants and patients with carotid atherosclerotic stenosis and found that the PG value of patients with stenosis was low (51). From this, it is not possible to determine whether a low PG value causes plaque formation; rather, this can only suggest that the PG value is lower after plaque formation. A different study using 4D flow MRI to assess the correlation between carotid hemodynamics and age in healthy adults observed that the PG value decreased with age, with old age being one of the risk factors for atherosclerotic plaque formation, which indirectly shows that low PG value can promote plaque formation (52).

The major highlight of our study was that 4D flow MRI technology was used to obtain comprehensive hemodynamic parameters of the carotid artery and was demonstrated to be capable of visualizing the direction and condition of blood flow, which has a degree of clinical relevance. Moreover, we not only examined the hemodynamic factors that affect the formation of carotid plaque but also evaluated geometric factors.

Despite these findings, some limitations to our study were present and should be addressed. First, we employed a cross-sectional design and measured hemodynamics based on the presence or absence of plaque, which lacked longitudinal follow-up to determine whether low WSS and PG promote plaque formation. Second, we only measured a single plane and did not obtain data for multiple planes upstream and downstream of the plaque, while a variety of factors such as different locations of the plaque (e.g., outer wall, side wall) were not considered. Therefore, the measurement of WSS was insufficiently detailed. The ability to measure WSS *in vivo* has long been a goal of clinical research, but most techniques do not have sufficient spatial resolution near the artery wall to make

an accurate measurement. Third, prior to the start of this study, although PASS software was used to calculate the sample size and the sample size of the study met the set requirements, we believe the sample to be insufficiently large. A large amount of 4D flow MRI data from multiple centers are needed for further validation. Future research addressing these limitations will contribute to a more comprehensive understanding of the geometric and hemodynamic factors related to the formation of carotid artery plaques.

Conclusions

As an initial and exploratory study, this work showed that a large bifurcation angle and low tortuosity of the carotid artery are geometric risk factors for plaque formation in this area. Low WSS and low PG are associated with carotid atherosclerotic plaque formation.

Acknowledgments

Funding: This study was funded by the Scientific Research Cultivation Plan of Cuiying Students in Lanzhou University Second Hospital (No. CYXZ2021-33), the National Natural Science Foundation of China (No. 81960309), and the Gansu Province Clinical Research Center for Functional and Molecular Imaging (No. 21JR7RA438).

Footnote

Reporting Checklist: The authors have completed the STROBE reporting checklist. Available at https://qims.amegroups.com/article/view/10.21037/qims-23-1827/rc

Conflicts of Interest: All authors have completed the ICMJE uniform disclosure form (available at https://qims.amegroups.com/article/view/10.21037/qims-23-1827/coif). The authors have no conflicts of interest to declare.

Ethical Statement: The authors are accountable for all aspects of the work in ensuring that questions related to the accuracy or integrity of any part of the work are appropriately investigated and resolved. This study was conducted in accordance with the Declaration of Helsinki (as revised in 2013) and was approved by the Ethics Committee of the Second Hospital of Lanzhou University (No. 2024A-616). Informed consent was taken from all participants.

References

1. Liu Z, Xin H, Chopp M. Axonal remodeling of the corticospinal tract during neurological recovery after stroke. Neural Regen Res 2021;16:939-43.
2. Song JW, Wasserman BA. Vessel wall MR imaging of intracranial atherosclerosis. Cardiovasc Diagn Ther 2020;10:982-93.
3. Shi Z, Li J, Zhao M, Peng W, Meddings Z, Jiang T, Liu Q, Teng Z, Lu J. Quantitative Histogram Analysis on Intracranial Atherosclerotic Plaques: A High-Resolution Magnetic Resonance Imaging Study. Stroke 2020;51:2161-9.
4. Zdun M, Ruszkowski JJ, Hetman M, Felsmann MZ. Head arteries of the red squirrel (Sciurus vulgaris). Vet Res Commun 2023;47:723-9.
5. Chang RW, Tucker LY, Rothenberg KA, Lancaster E, Faruqi RM, Kuang HC, Flint AC, Avins AL, Nguyen-Huynh MN. Incidence of Ischemic Stroke in Patients With Asymptomatic Severe Carotid Stenosis Without Surgical Intervention. JAMA 2022;327:1974-82.
6. Li H, Cao Z, Wang L, Liu C, Lin H, Tang Y, Yao P. Macrophage Subsets and Death Are Responsible for Atherosclerotic Plaque Formation. Front Immunol 2022;13:843712.
7. Zhang L, Li X, Lyu Q, Shi G. Imaging diagnosis and research progress of carotid plaque vulnerability. J Clin Ultrasound 2022;50:905-12.
8. Gottesman RF, Hao Q. Atherosclerosis all around: no plaque is innocent. Lancet Neurol 2023;22:286-8.
9. Ando T, Sekine T, Murai Y, Orita E, Takagi R, Amano Y, Iwata K, Nakaza M, Ogawa M, Obara M, Kumita SI. Multiparametric flow analysis using four-dimensional flow magnetic resonance imaging can detect cerebral hemodynamic impairment in patients with internal carotid artery stenosis. Neuroradiology 2020;62:1421-31.
10. Gupta AN, Markl M, Elbaz MSM. Intracardiac

and Vascular Hemodynamics with Cardiovascular Magnetic Resonance in Heart Failure. Heart Fail Clin 2021;17:135-47.
11. Zha X, Liang Z, Zheng L, Xu Y. Association of Cerebral Hemodynamics and Cognitive Function in Adult Patients with Moyamoya Disease: A Three-Dimensional Pseudo-Continuous Arterial Spin Labeling Study. World Neurosurg 2023;175:e447-54.
12. Wang M, Yang Y, Zhang W, Zhou F, Zhang X, Zhang J, Zhang B. Risk Factors for Cerebrovascular Events in Moyamoya Angiopathy Using 4D Flow MRI: A Pilot Study. J Magn Reson Imaging 2023;58:61-8.
13. Sotelo J, Dux-Santoy L, Guala A, Rodríguez-Palomares J, Evangelista A, Sing-Long C, Urbina J, Mura J, Hurtado DE, Uribe S. 3D axial and circumferential wall shear stress from 4D flow MRI data using a finite element method and a laplacian approach. Magn Reson Med 2018;79:2816-23.
14. Wåhlin A, Eklund A, Malm J. 4D flow MRI hemodynamic biomarkers for cerebrovascular diseases. J Intern Med 2022;291:115-27.
15. Steinman DA. Image-based computational fluid dynamics modeling in realistic arterial geometries. Ann Biomed Eng 2002;30:483-97.
16. Taylor CA, Steinman DA. Image-based modeling of blood flow and vessel wall dynamics: applications, methods and future directions: Sixth International Bio-Fluid Mechanics Symposium and Workshop, March 28-30, 2008 Pasadena, California. Ann Biomed Eng 2010;38:1188-203.
17. Chang GH, Schirmer CM, Modarres-Sadeghi Y. A reduced-order model for wall shear stress in abdominal aortic aneurysms by proper orthogonal decomposition. J Biomech 2017;54:33-43.
18. Lin S, Han X, Bi Y, Ju S, Gu L. Fluid-Structure Interaction in Abdominal Aortic Aneurysm: Effect of Modeling Techniques. Biomed Res Int 2017;2017:7023078.
19. Bissell MM, Raimondi F, Ait Ali L, Allen BD, Barker AJ, Bolger A, et al. 4D Flow cardiovascular magnetic resonance consensus statement: 2023 update. J Cardiovasc Magn Reson 2023;25:40.
20. Zhang Y, Ma C, Liang S, Li C, Zhu H, Li Z, Miao Z, Tong X, Dong K, Jiang C, Sui B, Mo D. Estimation of venous sinus pressure drop in patients with idiopathic intracranial hypertension using 4D-flow MRI. Eur Radiol 2023;33:2576-84.
21. Morbiducci U, Kok AM, Kwak BR, Stone PH, Steinman DA, Wentzel JJ. Atherosclerosis at arterial bifurcations: evidence for the role of haemodynamics and geometry. Thromb Haemost 2016;115:484-92.
22. Strecker C, Krafft AJ, Kaufhold L, Hüllebrandt M, Weber S, Ludwig U, Wolkewitz M, Hennemuth A, Hennig J, Harloff A. Carotid geometry is an independent predictor of wall thickness - a 3D cardiovascular magnetic resonance study in patients with high cardiovascular risk. J Cardiovasc Magn Reson 2020;22:67.
23. Zamani M, Skagen K, Scott H, Russell D, Skjelland M. Advanced ultrasound methods in assessment of carotid plaque instability: a prospective multimodal study. BMC Neurol 2020;20:39.
24. Leung TW, Wang L, Zou X, Soo Y, Pu Y, Ip HL, et al. Plaque morphology in acute symptomatic intracranial atherosclerotic disease. J Neurol Neurosurg Psychiatry 2020;92:370-6.
25. Fabiani I, Palombo C, Caramella D, Nilsson J, De Caterina R. Imaging of the vulnerable carotid plaque: Role of imaging techniques and a research agenda. Neurology 2020;94:922-32.
26. Schinkel AFL, Bosch JG, Staub D, Adam D, Feinstein SB. Contrast-Enhanced Ultrasound to Assess Carotid Intraplaque Neovascularization. Ultrasound Med Biol 2020;46:466-78.
27. Strecker C, Krafft AJ, Kaufhold L, Hüllebrandt M, Treppner M, Ludwig U, Köber G, Hennemuth A, Hennig J, Harloff A. Carotid Geometry and Wall Shear Stress Independently Predict Increased Wall Thickness-A Longitudinal 3D MRI Study in High-Risk Patients. Front Cardiovasc Med 2021;8:723860.
28. Bijari PB, Wasserman BA, Steinman DA. Carotid bifurcation geometry is an independent predictor of early wall thickening at the carotid bulb. Stroke 2014;45:473-8.
29. Phan TG, Beare RJ, Jolley D, Das G, Ren M, Wong K, Chong W, Sinnott MD, Hilton JE, Srikanth V. Carotid artery anatomy and geometry as risk factors for carotid atherosclerotic disease. Stroke 2012;43:1596-601.
30. Cibis M, Potters WV, Selwaness M, Gijsen FJ, Franco OH, Arias Lorza AM, de Bruijne M, Hofman A, van der Lugt A, Nederveen AJ, Wentzel JJ. Relation between wall shear stress and carotid artery wall thickening MRI versus CFD. J Biomech 2016;49:735-41.
31. Zalud NC, Bulusu KV, Plesniak MW. Shear stress metrics associated with pro-atherogenic high-risk anatomical features in a carotid artery bifurcation model. Clin Biomech (Bristol, Avon) 2023;105:105956.
32. Wild NC, Bulusu KV, Plesniak MW. Vortical Structures Promote Atheroprotective Wall Shear Stress Distributions

in a Carotid Artery Bifurcation Model. Bioengineering (Basel) 2023;10:1036.
33. Jiang P, Chen Z, Hippe DS, Watase H, Sun B, Lin R, Yang Z, Xue Y, Zhao X, Yuan C. Association Between Carotid Bifurcation Geometry and Atherosclerotic Plaque Vulnerability: A Chinese Atherosclerosis Risk Evaluation Study. Arterioscler Thromb Vasc Biol 2020;40:1383-91.
34. Gallo D, Steinman DA, Bijari PB, Morbiducci U. Helical flow in carotid bifurcation as surrogate marker of exposure to disturbed shear. J Biomech 2012;45:2398-404.
35. Corban MT, Eshtehardi P, Suo J, McDaniel MC, Timmins LH, Rassoul-Arzrumly E, Maynard C, Mekonnen G, King S 3rd, Quyyumi AA, Giddens DP, Samady H. Combination of plaque burden, wall shear stress, and plaque phenotype has incremental value for prediction of coronary atherosclerotic plaque progression and vulnerability. Atherosclerosis 2014;232:271-6.
36. Saho T, Onishi H. Evaluation of the impact of carotid artery bifurcation angle on hemodynamics by use of computational fluid dynamics: a simulation and volunteer study. Radiol Phys Technol 2016;9:277-85.
37. De Nisco G, Kok AM, Chiastra C, Gallo D, Hoogendoorn A, Migliavacca F, Wentzel JJ, Morbiducci U. The Atheroprotective Nature of Helical Flow in Coronary Arteries. Ann Biomed Eng 2019;47:425-38.
38. Ren L, Xu R, Zhao C, Li W, Wang S, Cao C, Gong Y, Zhu J, Feng X, Ren B, Xia S. Tortuosity and Proximal-Specific Hemodynamics Associated with Plaque Location in the Carotid Bulb Stenosis. J Vasc Res 2023;60:160-71.
39. Sullivan TM, Zeller T, Nakamura M, Caro CG, Lichtenberg M. Swirling Flow and Wall Shear: Evaluating the BioMimics 3D Helical Centerline Stent for the Femoropopliteal Segment. Int J Vasc Med 2018;2018:9795174.
40. Dong X, Yuan X, Wang L, Liu J, Midgley AC, Wang Z, Wang K, Liu J, Zhu M, Kong D. Construction of a bilayered vascular graft with smooth internal surface for improved hemocompatibility and endothelial cell monolayer formation. Biomaterials 2018;181:1-14.
41. Ding Z, Fan Y, Deng X, Zhan F, Kang H. Effect of swirling flow on the uptakes of native and oxidized LDLs in a straight segment of the rabbit thoracic aorta. Exp Biol Med (Maywood) 2010;235:506-13.
42. Gallo D, Bijari PB, Morbiducci U, Qiao Y, Xie YJ, Etesami M, Habets D, Lakatta EG, Wasserman BA, Steinman DA. Segment-specific associations between local haemodynamic and imaging markers of early atherosclerosis at the carotid artery: an in vivo human study. J R Soc Interface 2018;15:20180352.
43. El Sayed R, Sharifi A, Park CC, Haussen DC, Allen JW, Oshinski JN. Optimization of 4D Flow MRI Spatial and Temporal Resolution for Examining Complex Hemodynamics in the Carotid Artery Bifurcation. Cardiovasc Eng Technol 2023;14:476-88.
44. Han D, Starikov A, Ó Hartaigh B, Gransar H, Kolli KK, Lee JH, Rizvi A, Baskaran L, Schulman-Marcus J, Lin FY, Min JK. Relationship Between Endothelial Wall Shear Stress and High-Risk Atherosclerotic Plaque Characteristics for Identification of Coronary Lesions That Cause Ischemia: A Direct Comparison With Fractional Flow Reserve. J Am Heart Assoc 2016;5:e004186.
45. Cho KI, Kim BH, Kim HS, Heo JH. Low Carotid Artery Wall Shear Stress is Associated with Significant Coronary Artery Disease in Patients with Chest Pain. J Atheroscler Thromb 2016;23:297-308.
46. Carallo C, Tripolino C, De Franceschi MS, Irace C, Xu XY, Gnasso A. Carotid endothelial shear stress reduction with aging is associated with plaque development in twelve years. Atherosclerosis 2016;251:63-9.
47. Roustaei M, Nikmaneshi MR, Firoozabadi B. Simulation of Low Density Lipoprotein (LDL) permeation into multilayer coronary arterial wall: Interactive effects of wall shear stress and fluid-structure interaction in hypertension. J Biomech 2018;67:114-22.
48. Li CH, Gao BL, Wang JW, Liu JF, Li H, Yang ST. Hemodynamic Factors Affecting Carotid Sinus Atherosclerotic Stenosis. World Neurosurg 2019;121:e262-76.
49. Zhang G, Zhang S, Qin Y, Fang J, Tang X, Li L, Zhou Y, Wu D, Yan S, Liu WV, Zhu W. Differences in Wall Shear Stress Between High-Risk and Low-Risk Plaques in Patients With Moderate Carotid Artery Stenosis: A 4D Flow MRI Study. Front Neurosci 2021;15:678358.
50. Domanin M, Gallo D, Vergara C, Biondetti P, Forzenigo LV, Morbiducci U. Prediction of Long Term Restenosis Risk After Surgery in the Carotid Bifurcation by Hemodynamic and Geometric Analysis. Ann Biomed Eng 2019;47:1129-40.
51. Jia L, Hua Y, Jiao L, Ma Y, Xing Y, Wang L, Hui P, Pan X, Fang Y, Peng T, Meng X, Zhu H, Wu C, Yan Y, Han B, Yang J, Zhang N, Zhang K, Xu D. Effects of plaque characteristics and artery hemodynamics on the residual stenosis after carotid artery stenting. J Vasc Surg

2023;78:430-437.e4.
52. Zhang G, Wang Z, Zhang S, Qin Y, Yao Y, Tang X, Li L, Zhou Y, Wu D, Chaudhary N, Liu WV, Zhu W. Age and anatomical location related hemodynamic changes assessed by 4D flow MRI in the carotid arteries of healthy adults. Eur J Radiol 2020;128:109035.

Cite this article as: Han N, Wang J, Ma Y, Ma L, Zheng Y, Fan F, Wu C, Yue S, Li J, Liang J, Zhang H, Zhou Y, Yang T, Zhang J. The hemodynamic and geometric characteristics of carotid artery atherosclerotic plaque formation. Quant Imaging Med Surg 2024;14(7):4348-4361. doi: 10.21037/qims-23-1827

